AGU PUBLICATIONS

JGR

Journal of Geophysical Research: Atmospheres

RESEARCH ARTICLE
10.1002/2015JD024230

Key Points:
- A subgrid orographic parameterization for global atmospheric forecast models is updated
- The effects of orography anisotropy and flow-blocking drag are additionally parameterized
- The parameterization improves the forecast skills in the Global/Regional Integrated Model system

Correspondence to:
H.-J. Choi,
hj.choi@kiaps.org

Citation:
Choi, H.-J., and S.-Y. Hong (2015), An updated subgrid orographic parameterization for global atmospheric forecast models, *J. Geophys. Res. Atmos.*, *120*, 12,445–12,457, doi:10.1002/2015JD024230.

Received 16 SEP 2015
Accepted 25 NOV 2015
Accepted article online 27 NOV 2015
Published online 22 DEC 2015

An updated subgrid orographic parameterization for global atmospheric forecast models

Hyun-Joo Choi[1] and Song-You Hong[1]

[1]Korea Institute of Atmospheric Prediction Systems, Seoul, South Korea

Abstract A subgrid orographic parameterization (SOP) is updated by including the effects of orographic anisotropy and flow-blocking drag (FBD). The impact of the updated SOP on short-range forecasts is investigated using a global atmospheric forecast model applied to a heavy snowfall event over Korea on 4 January 2010. When the SOP is updated, the orographic drag in the lower troposphere noticeably increases owing to the additional FBD over mountainous regions. The enhanced drag directly weakens the excessive wind speed in the low troposphere and indirectly improves the temperature and mass fields over East Asia. In addition, the snowfall overestimation over Korea is improved by the reduced heat fluxes from the surface. The forecast improvements are robust regardless of the horizontal resolution of the model between T126 and T510. The parameterization is statistically evaluated based on the skill of the medium-range forecasts for February 2014. For the medium-range forecasts, the skill improvements of the wind speed and temperature in the low troposphere are observed globally and for East Asia while both positive and negative effects appear indirectly in the middle-upper troposphere. The statistical skill for the precipitation is mostly improved due to the improvements in the synoptic fields. The improvements are also found for seasonal simulation throughout the troposphere and stratosphere during boreal winter.

1. Introduction

The parameterization of the effects of subgrid-scale orography in global numerical weather prediction and climate models is crucial for successful weather and climate predictions [e.g., *Palmer et al.,* 1986; *Miller et al.,* 1989]. Subgrid orographic parameterizations (SOPs) describe the transport of momentum induced by subgrid-scale orography to large-scale flow. Considerable efforts have been made to more realistically parameterize this orography-induced force (i.e., subgrid orographic drag) (for a review, see *Kim et al.* [2003] and *Alexander et al.* [2010]).

In general, subgrid orographic drag is classified into three types: Drag due to gravity waves (GWs), low-level wave breaking, and flow blocking [*Zadra et al.,* 2003, Figure 1; *Kim and Doyle*, 2005]. The GWs generated by flow over mountains propagate vertically and produce drag at upper levels when breaking, which is known as GW drag (GWD). The low-level breaking and trapped leewaves downstream can enhance drag in the lower troposphere. The flow-blocking drag (FBD) is forced by flow blocked on the mountain flanks or flowing around the mountain under upstream stable conditions, providing drag near the surface, where the blocking occurs.

Initially, SOPs concentrated mainly on parameterizing the effects of GWD and were based on the two-dimensional (2-D) linear GW theory for an idealized mountain [e.g., *Boer et al.,* 1984; *McFarlane*, 1987]. The GWD parameterizations led to substantial improvements in lower stratosphere and troposphere simulations, such as the separation of the subtropical and polar night jets and the alleviation of the surface westerlies [*Palmer et al.,* 1986]. Since then, SOPs have been improved to include more sophisticated orographic effects, such as the aforementioned low-level wave breaking [e.g., *Kim and Arakawa*, 1995; *Hong et al.,* 2008] and flow blocking [e.g., *Lott and Miller*, 1997; *Scinocca and McFarlane*, 2000; *Webster et al.,* 2003; *Kim and Doyle*, 2005], as well as orographic specifications, such as orographic anisotropy [e.g., *Gregory et al.,* 1998; *Scinocca and McFarlane*, 2000; *Kim and Doyle*, 2005]. The inclusion of drag effects enhanced by low-level wave breaking improved the forecasts of weather phenomena, such as extra tropical cyclones [*Hong et al.,* 2008] and climate simulations [*Kim*, 1996; *Gregory et al.,* 1998]. The FBD parameterizations improved the simulations of the wind fields over the troposphere and lower stratosphere [*Zadra et al.,* 2003] and other fields indirectly affected, such as precipitation [*Zhong and Chen*, 2015].

In this study, the SOP from *Hong et al.* [2008] based on *Kim and Arakawa* [1995] implemented in the Global/Regional Integrated Model system (GRIMs), including the drag effects associated with 2-D GWs and low-level wave breaking, is updated by including the effects of 3-D orographic anisotropy and FBD. The impact of the updated SOP on short-range forecasts is investigated for a heavy snowfall event over East Asia using the GRIMs global model program (GMP). The parameterization is statistically evaluated based on the skill of medium-range forecasts, and its impacts on seasonal simulations are also examined during boreal winter. One may argue that the SOP used in this study is out of date. However, it is natural to revise an existing physics component on a well-established forecast model such as the GRIMs. Thus, our starting point is the GWD from *Hong et al.* [2008] and FBD based on the *Kim and Doyle* [2005]. In addition, several modifications/new formulations are introduced to both GWD and FBD.

This paper is organized as follows: Section 2 describes the model, SOP, and experimental design; section 3 presents the impact of the updated SOP on short- and medium-range forecasts and seasonal simulations; and section 4 presents a summary and conclusions.

2. Model and Experimental Design

2.1. Model Description

The model used in this study is the GRIMs-GMP [*Hong et al.,* 2013] based on the National Centers for Environmental Prediction seasonal forecast model [*Kanamitsu et al.,* 2002]. The GRIMs has been developed for numerical weather prediction, seasonal forecasts, and climate research projects for global-regional scales with improved model dynamics and physics. The model includes two options in the dynamical core (spherical harmonics and double Fourier series) and multiple options for each physics parameterization. In this study, we utilize the spherical harmonics dynamical core, which is widely used in global atmospheric models with high numerical accuracy and stability, and the physics package according to Table 1 from *Hong et al.* [2013] with several minor revisions (e.g., the deep convective scheme from *Lim et al.* [2014]). The SOP scheme is updated as described in the next subsection.

2.2. Subgrid Orographic Parameterization (SOP)

The GRIMs uses the SOP from *Hong et al.* [2008] based on *Kim and Arakawa* [1995], which includes the effects of the GWD and the drag due to low-level wave breaking and nonhydrostatic wave trapping (OGWD). In this study, the parameterization is updated by also including the effects of orographic anisotropy and the FBD.

First, the formulations for the OGWD parameterization are extended to include the effects of orographic anisotropy according to *Kim and Doyle* [2005]. To achieve this, the orographic direction (OD), which is equivalent to the horizontal aspect ratio of the orography, is introduced as

$$\mathrm{OD} \equiv \frac{L_x^{\perp}}{L_x}, \tag{1}$$

where L_x is the effective orographic length, which represents the subgrid-scale mountain width in the direction of low-level wind measured at the critical orographic height. The $L_x^{\perp}$ denotes L_x for the cross-wind direction. The Froude number, one of the factors that determines the GW stress at a reference level, is then redefined through multiplication with OD as follows:

$$Fr_0 \equiv h\frac{N_0}{U_0}\,\mathrm{OD}, \tag{2}$$

where h is the orographic height, which is defined as the standard deviation of subgrid-scale orography; N_0 is the low-level Brunt-Väisälä frequency; and U_0 is the low-level horizontal wind speed. The GW stress (τ_{GWD}) at the reference level is given as follows:

$$\tau_{\mathrm{GWD}} = \rho_0 E\,\frac{m}{\lambda_{\mathrm{eff}}}\,G\frac{|U_0|^3}{N_0}, \tag{3}$$

$$\mathrm{E} \equiv (\mathrm{OA}+2)^{C_E Fr_0/Fr_c}, \quad m \equiv (1+L_x)^{OA+1}, \quad G \equiv \frac{Fr_0^2}{Fr_0^2 + C_G \mathrm{OC}^{-1}}, \tag{4}$$

where ρ_0 is the low-level density; E is the enhancement factor for representing the nonlinear enhancement of drag due to the low-level wave breaking, which is calculated by the orographic asymmetry (OA), which

represents the shape and location of subgrid-scale orography relative to the grid and the Fr_0 normalized by its critical value ($Fr_c = 1$); m is the number of subgrid-scale orography; λ_{eff} is the effective grid length; G is an asymptotic function that provides a smooth transition between the nonblocking and blocking cases and includes the effect of orographic convexity (OC) corresponding to the vertical orographic aspect ratio; and C_E and C_G are set to 0.8 and 0.5, respectively, based on the mesoscale simulation results from *Kim and Arakawa* [1995]. A more detailed description is given by *Kim and Doyle* [2005]. The GW stress is the same as that of *Hong et al.* [2008] except for the Fr_0, including the effect of OD and a free parameter, λ_{eff}. In *Hong et al.* [2008], the λ_{eff} was practically set to the grid length with a minimum limit of 50 km, whereas in this study, it is set to twice the grid length without the limit. The updated λ_{eff} has little effect on the short- and medium-range forecasts but gives slightly better seasonal forecast skills.

Second, the FBD effects are included in the OGWD parameterization. The flow-blocking stress is given as follows:

$$\tau_{\text{FBD}} = \frac{1}{2}\rho_0 \frac{m}{\Delta_x^2} C_d \Delta_x^{\perp} L_x^{\perp} h_B |U_0|^2, \tag{5}$$

where Δ_x^2 is the grid box area, C_d is the bulk drag coefficient of order unity, $\Delta_x^{\perp}$ is the grid length in the cross-wind direction, and h_B is the height of the blocked layer. The FBD parameterization generally follows the study of *Kim and Doyle* [2005], except for the h_B and C_d. *Kim and Doyle* [2005] define h_B as a function of the Froude number $\left(\equiv \frac{U_0}{N_0}(Fr_0 - Fr_c) > 0 \right)$, whereas we determine it according to the dividing streamline theory [*Snyder et al.*, 1985; *Etling*, 1989], as in *Zhong and Chen* [2015], who state that the blocked layer occurs when the potential energy exceeds the kinetic energy. Thus, h_B is found by solving the following equation:

$$\int_{h_B}^{H} N^2(z)(H - z)\, \mathrm{d}z = \frac{U^2(h_B)}{2} \tag{6}$$

where H is the maximum height of the actual subgrid orography within each grid box and N and U are the basic-state static stability and wind, respectively. C_d is theoretically set to 1 by *Kim and Doyle* [2005], but this is inconsistent with the observations, which show its orographic aspect ratio dependence [*Batchelor*, 1967]. Therefore, according to *Lott and Miller* [1997], we calculate C_d as a function of OD:

$$C_d = \max\left\{2 - \frac{1}{\text{OD}}, 0\right\} \tag{7}$$

C_d is approximately 1 for isotropic orography, 2 for flow orthogonal to an elongated orography, and 0 for flow along an elongated orography.

2.3. Experimental Setup

Short- and medium-range forecasts and seasonal simulations are performed using the GRIMs-GMP with original (CTL experiment) and updated (SOP experiment) SOPs. Because the effects of SOP are significant mainly in winter, as in previous studies [e.g., *Zadra et al.*, 2003] we focus on high-impact weather, such as heavy snowfall events over South Korea during boreal winter. For the short-range forecasts, a record-breaking heavy snowfall event that occurred over South Korea on 4 January 2010 is selected, and the impact of the updated SOP on the synoptic fields and precipitation is investigated by comparing the SOP and CTL results. The model is integrated for 48 h, starting from 00:00 UTC 3 January 2010, using initial and boundary conditions from the National Centers for Environmental Prediction (NCEP) Global Forecast System (GFS) analysis [*Kanamitsu*, 1989]. We focus on the model results with a resolution of T510L64. The effects of the updated SOP on the horizontal resolution are investigated by comparing the experiments with T126, T254, and T510 resolutions, which correspond to the grid spacing of approximately 100, 50, and 25 km, respectively. We also perform the following four additional experiments to investigate the individual impacts of the factors updated in SOP: (i) An SOPA experiment with the orographic anisotropy effect only, (ii) an SOPF experiment with the flow-blocking drag effect only, (iii) SOPH, and (iv) SOPB experiments that are the same as the SOP experiment except for the use of the original height of the blocked layer (i.e., $h_B \equiv \frac{U_0}{N_0}(F_{r0} - F_{rc}) > 0$) and bulk drag coefficient (i.e., $C_d = 1$), respectively.

For the medium-range forecasts, 28-member ensembles of 10 day forecasts at a resolution of T214L64 are performed using initial and boundary data from the NCEP GFS analysis for every 00:00 UTC in February 2014,

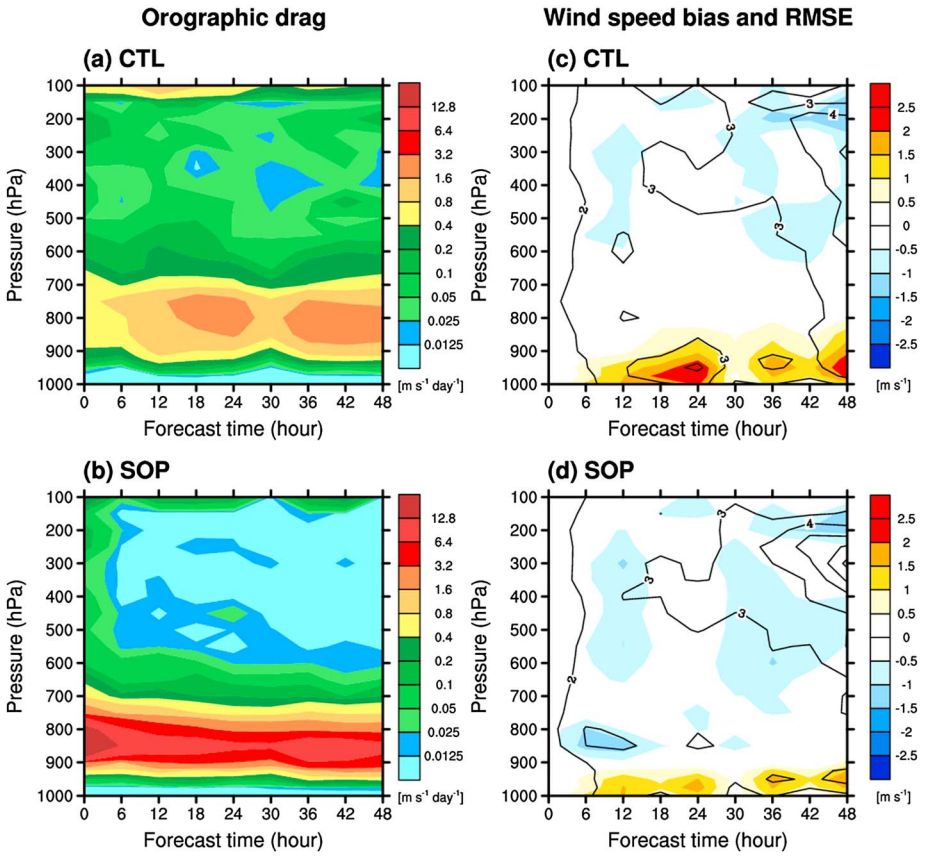

Figure 1. Time-pressure cross sections of the (a, b) subgrid orographic drag averaged over East Asia and (c, d) biases (shaded) and RMSEs (contours) of the wind speed computed against the FNL data averaged over the East Asian continent from the (Figures 1a and 1c) CTL and (Figures 1b and 1d) SOP experiments.

when an anomalously long-lasting heavy snowfall event over South Korea occurred. The medium-range forecasts with a number of members are performed at a lower horizontal resolution (T214) compared with the short-range forecasts (T510) because of the limited computational resources. The synoptic features from the CTL and SOP experiments are statistically evaluated based on the forecast skill regarding the bias and root-mean-square error (RMSE) of the simulated wind speed and temperature computed against the radiosonde data.

The seasonal simulations consisting of five-member ensembles are performed for the boreal winter from December–February (DJF) in the years 2013–2014 when the seasonal mean states are shown to be similar to climatology under the normal sea surface temperatures (SSTs). The ensemble runs are initialized at 0000 UTC 1–5 November with initial conditions derived from the NCEP GFS analysis data. As for the surface boundary condition, Optimum Interpolation Sea Surface Temperature data [*Reynolds et al.,* 2007] are used. The horizontal resolution of the model for the seasonal simulation is T126, and the vertical resolution is the same as that for the short- and medium-range forecasts. Through the comparison between the seasonal simulations for the CTL and SOP experiments, the impacts of the updated SOP on the seasonal predictability of zonal mean zonal wind and temperature, stationary eddy, and precipitation are examined.

3. Results

3.1. Short-Range Forecasts

Figures 1a and 1b show the subgrid orographic drag $\left(\sqrt{(dU/dt)^2 + (dV/dt)^2}\right)$ averaged over East Asia (25°–50°N and 105°–145°E) from the CTL and SOP experiments during the 48 h forecast (00:00 UTC 3–5 January 2010) for a heavy snowfall event over Korea. The comparison between the two experiments shows that the

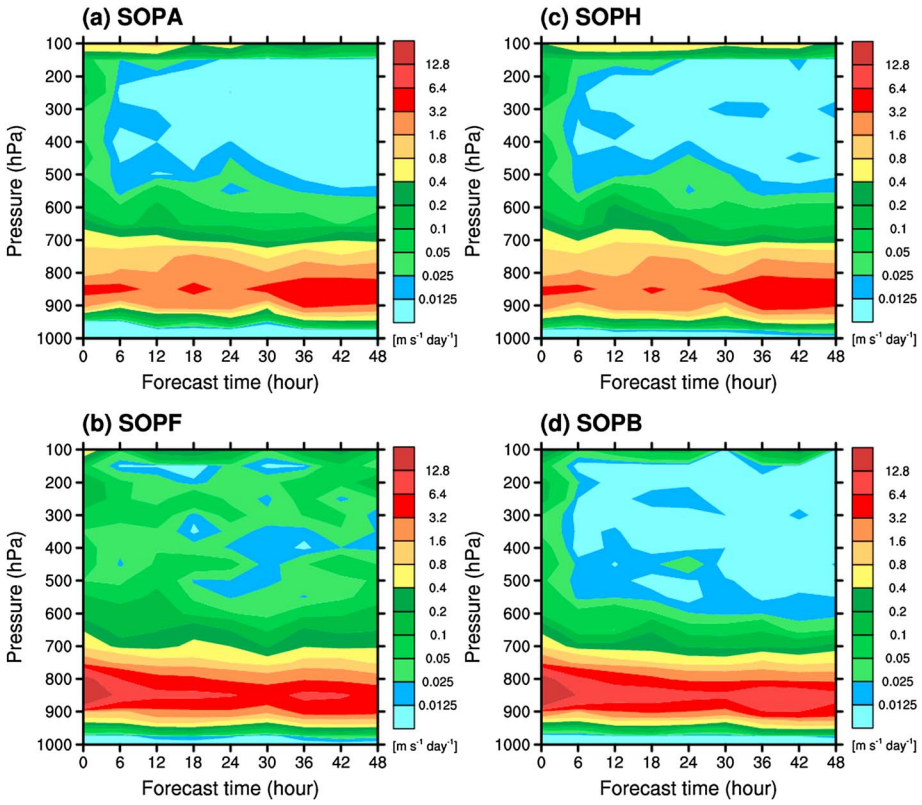

Figure 2. Time-pressure cross sections of the subgrid orographic drag averaged over East Asia from the (a) SOPA, (b) SOPF, (c) SOPH, and (d) SOPB experiments.

orographic drag clearly increases (more than fourfold) in the low troposphere when the SOP is updated. The orographic drag in the middle–upper troposphere is slightly decreased by the reduced OGWD, though not as significantly as for the low troposphere. Figures 1c and 1d show the biases and RMSEs of the wind speed averaged over the East Asian continent from the CTL and SOP experiments. The skill scores are calculated through comparison with the NCEP Final Analysis (FNL) data, which is presented on $1° \times 1°$ grids for every 6 h. The results demonstrate that the enhanced drag in the low troposphere from the SOP experiment alleviates the low-tropospheric wind speed overestimation over the East Asian continent from the CTL experiment. Note that the orographic drag has an opposite sign to the wind, causing its deceleration. Its magnitude is shown in Figures 1a and 1b. The wind reduction in the low troposphere improves the forecast skills for the low-tropospheric wind, with a substantially reduced bias and RMSE for the SOP experiment. However, the updated orographic drag induces negative effects (i.e., degradation of skills) indirectly in some regions, especially in the middle-upper troposphere in spite of the small magnitude of the drag. The deficiency may need to be improved by considering the interaction with other processes, which will be studied further in the future.

To understand the effects by updating the SOP, the individual impacts of each updated factor (i.e., orographic anisotropy, flow-blocking drag, height of the blocked layer, and bulk drag coefficient) are investigated in Figure 2, which show the orographic drag from the SOPA, SOPF, SOPH, and SOPB experiments, respectively. Figures 2a and 2b indicate that the reduced (enhanced) drag in the middle-upper (low) troposphere from the SOP experiment shown in Figure 1 is mainly because of the orographic anisotropy (additional flow-blocking drag). The orographic drag in the SOPH experiment with the original h_B is much smaller in the low troposphere than when the updated one is used. This is because the condition causing the flow-blocking effects (i.e., $F_{r0} - F_{rc} > 0$) is rarely met, and the magnitude of the h_B, which is one of factors that determines the magnitude of FBD, is smaller when the original h_B is used. The smaller drag in the SOPH experiment, in turn, leads to less wind improvement in the low troposphere. The orographic drag in the SOPB experiment is similar to that in the SOP experiment, implying that the flow-blocking effects on the short-range forecasts over East Asia are less sensitive to the C_d.

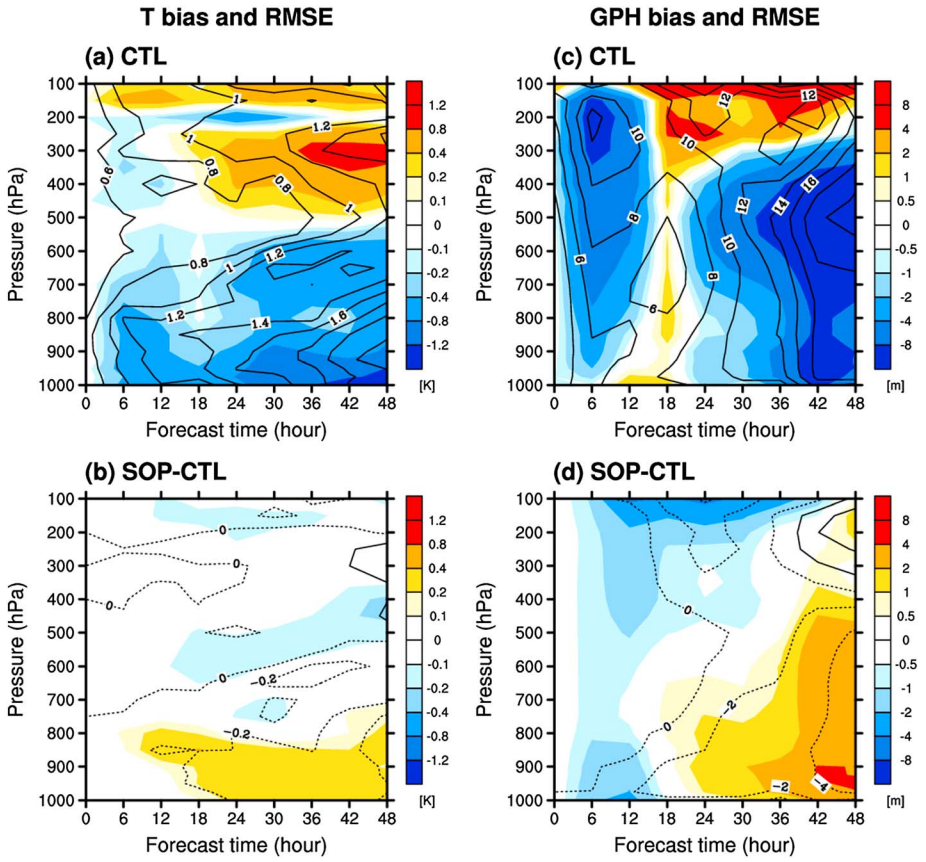

Figure 3. Time-pressure cross sections of the biases (shaded) and RMSEs (contours) of the (a, b) temperature and (c, d) geopotential height computed against the FNL data over East Asia from the (Figures 3a and 3c) CTL experiment and the (Figures 3b and 3d) differences in bias and RMSE between the SOP and CTL experiments.

The updated SOP does affect not only the wind but also other fields indirectly. Figure 3a shows the bias and RMSE of the average temperature over East Asia from the CTL experiment during the 48 h forecast, with cold (warm) biases for the low–middle (middle–upper) troposphere. The biases and RMSE increase with increasing forecast time, and the skill scores are worse for the low troposphere than for the middle–upper troposphere. Figure 3b shows the differences in the bias and RMSE of the temperatures from the SOP and CTL experiments. The bias difference (temperature difference) between the two experiments shows that the temperature in the low (middle–upper) troposphere is higher (lower) in the SOP than in the CTL experiment. The temperature differences are mostly out of phase with the CTL experiment biases, indicating their reduction in the SOP experiment. This bias reduction is particularly noticeable for the low troposphere, where the wind bias is substantially reduced by the enhanced orographic drag. Skill improvements are also found for the RMSE.

The temperature changes can be explained partly by the thermal wind relationship. In the low troposphere, the reduced wind in the SOP experiment causes a weakened horizontal gradient in temperature, which corresponds to warming over East Asia. This low-tropospheric warming expands the air mass responsible for the increase in geopotential height (Figure 3d). The positive differences in geopotential height indicate that the negative bias of the geopotential height in the CTL experiment (Figure 3c) is reduced in the SOP experiment. Skill improvements are found for the RMSE and bias. Although we focus on East Asia, the improvements in the wind, temperature, and geopotential height through updating the SOP are shown worldwide, except for in the summer hemisphere (not shown).

The improvements in the synoptic fields positively affect the precipitation forecast. Figure 4 shows the snowfall from the rain gauge observations and the CTL and SOP experiment simulations accumulated for 12 h (1800 UTC 3 January and 0600 UTC 4 January 2010), which nearly corresponds to the rainy period

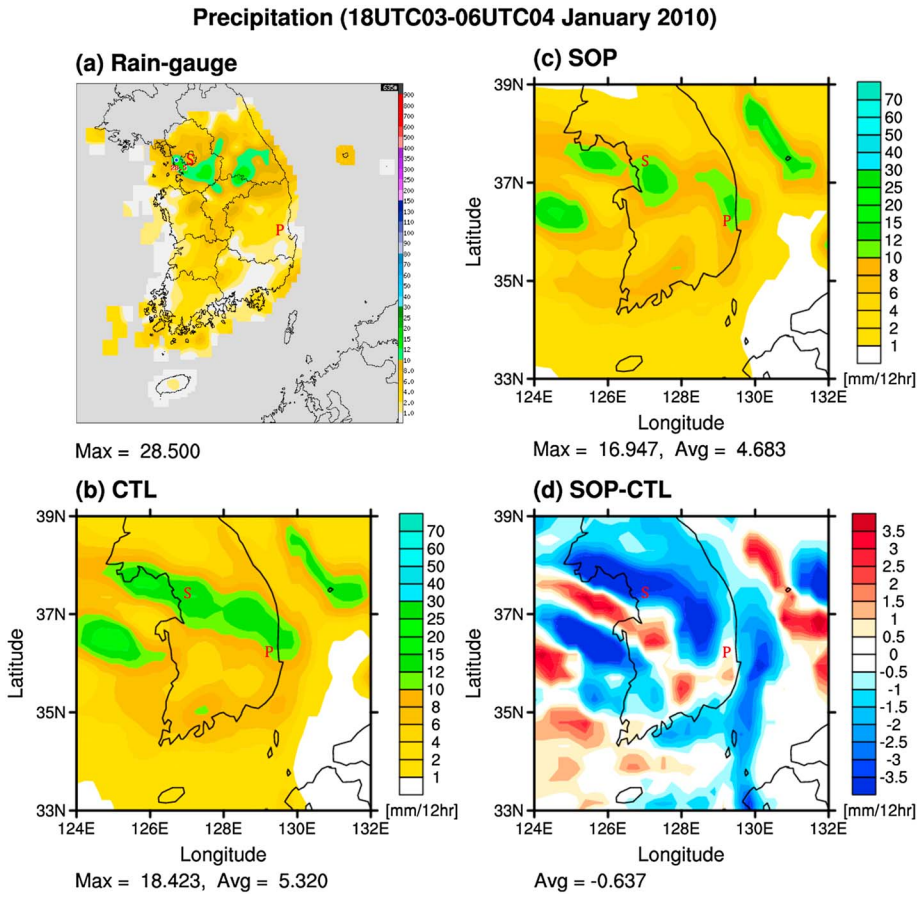

Figure 4. Twelve hour accumulated precipitation (mm) for 00:00 UTC 4 January 2010, obtained from the (a) rain gauge over South Korea, (b) CTL, and (c) SOP experiments and the (d) difference in precipitation between the SOP and CTL experiments. The capitals of S and P represent the locations of Seoul and Pohang.

over Korea. In Seoul (~37.5°N, ~127°E), heavy snowfall is observed with an accumulation of 28.5 mm. This is well-reproduced by the CTL and SOP experiments, although the maximum magnitude is underestimated. However, the overall snowfall is overestimated in the CTL experiment, especially around Pohang (~36°N, ~129.5°E), but improved in the SOP simulation by the reduced heat fluxes from the surface due to the decreased turbulent exchange coefficients resulting from the weakened surface wind. The improvement also can be induced dynamically by the reduced orographic lifting due to the reduced low-level wind.

The dependence of the effects of the updated SOP on the horizontal resolution of the model is investigated. Figure 5 shows the times series of the biases and RMSEs of the 10 m wind speed averaged over East Asia for the 48 h forecast (heavy snowfall event, 00:00 UTC, 3–5 January 2012) from the CTL and SOP experiments at resolutions of T126, T254, and T510. The skill scores from both experiments are computed against the FNL data. For the CTL experiment, the 10 m wind speed is overestimated compared with the FNL, and the positive biases are reduced as the resolution increases from T126 to T254. In contrast, the bias difference between T254 and T510 is not significant. The dependence of the skill score on the resolution is also consistent for the RMSE. When the SOP is updated, the excessive wind speed from the CTL experiment significantly decreases for all resolutions, although the bias slightly increases negatively for some periods for the T510 resolution. Similarly, the RMSE scores are improved for all SOP experiments compared with those of the CTL. However, the RMSE improvement for T510 is not larger than for the other resolutions, consistent with the negatively increased bias due to the excessive wind reduction for T510. Although the parameterized orographic drag decreases as the horizontal resolution increases (by approximately 5% from T126 to T510), the excessive reduction of winds at T510 can be caused by the nonlinear interactions of the orographic drag with other processes. The effects of the updated SOP over the whole troposphere at T254 and T126 are consistent with those at T510, shown in Figure 1.

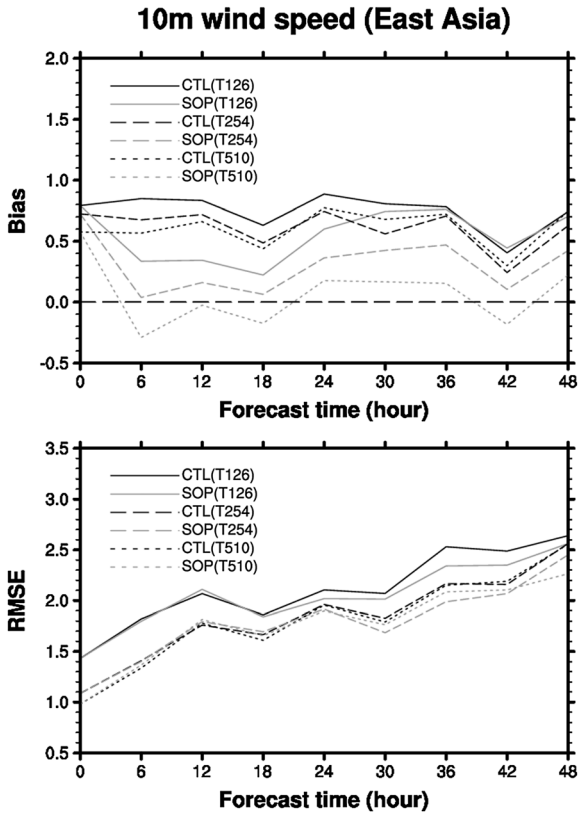

Figure 5. Time series of the (top) biases and (bottom) RMSEs of the 10 m wind speed computed against the FNL data averaged over East Asia from the CTL (black lines) and SOP (gray lines) experiments for the T126 (solid lines), T254 (dashed lines), and T510 (dotted lines) resolutions.

3.2. Medium-Range Forecasts

To statistically verify the updated SOP, the ensemble forecast skills for the wind speed and temperature are computed against the radiosonde data. The skill scores for the 10 day forecasts are averaged for February 2014. Figures 6a and 6c show the biases and RMSEs of the wind speed from the CTL simulation averaged over East Asia and globally. The bias patterns for the East Asian and global averages are similar to those of the short-range forecasts, mostly with an excessive (lower) wind speed for the low (middle–upper) troposphere. The bias and RMSE increase with increasing forecast time, especially for the middle–upper troposphere. Note that the low wind biases in the middle-upper troposphere do not imply the excessive orographic drag in the CTL experiment because its magnitude is small in the regions. Figures 6b and 6d show the differences in the bias and RMSE between the SOP and CTL experiments, with general improvement in the scores for the East Asian and global averages for the SOP experiment. For the early forecasts (~4 days), the wind improvements in the SOP experiment are noticeable in the low troposphere due to the directly enhanced orographic drag, which are consistent with those for the short-range forecasts. Although the skills are degraded in the middle-upper troposphere for the early forecasts, the improvements for the middle–upper troposphere become larger with increasing forecast time in spite of the small changes in orographic drag, perhaps because of forcing terms from other physical and dynamical processes being indirectly changed by the modified orographic drag, as shown by *Zadra et al.* [2003].

The wind improvement due to the updated SOP also improves the temperature prediction via the thermal wind relationship. Figures 7a and 7c show the East Asian and global forecast skill scores for the temperature bias and RMSE from the CTL experiment for the 10 day forecast averaged for February 2014. A cold bias is noticeable both globally and for East Asia, which is reduced by the updated SOP for the low and upper troposphere. Although for the middle-troposphere this bias is intensified in the SOP experiment, the RMSE is improved. The statistically significant improvements in forecast skills for the wind and temperature are observed over the whole boreal winter period (i.e., December to February).

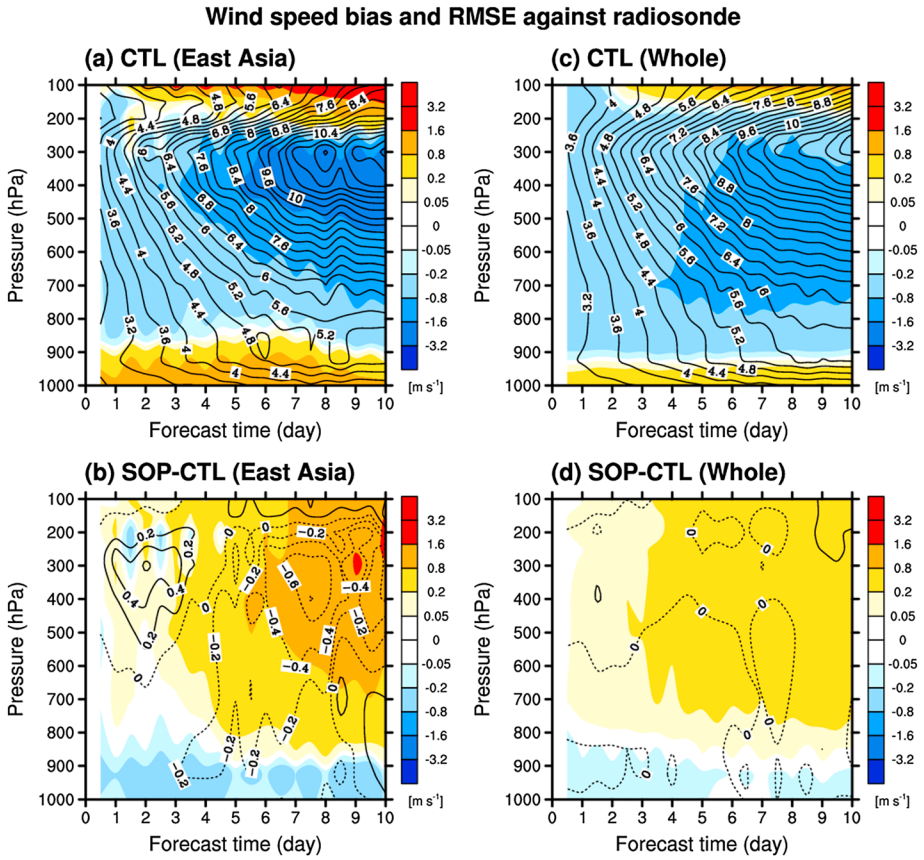

Figure 6. Time-pressure cross sections of the biases (shaded) and RMSEs (contours) of the wind speed computed against the radiosonde data averaged over (a, b) East Asia and (c, d) globally from the (Figures 6a and 6c) CTL experiment and the (Figures 6b and 6d) differences in bias and RMSE between the SOP and CTL experiments for February 2014.

In addition, it is found that the statistical skill for the precipitation during February 2014 is mostly improved in the SOP experiment due to the improvements in the synoptic fields. Figure 8 shows the equivalent threat scores (ETS) for 1 to 5 day forecasts from the CTL and SOP experiments averaged over February 2014. The skill scores are calculated against rain gauge observations over South Korea. In the SOP experiment, the ETS is mostly increased (i.e., improved) compared with that in the CTL experiment, which can be due to the changes in the surface flux or/and the amount of orographic lifting indirectly caused by updating the SOP, as discussed in the short-range forecasts.

3.3. Seasonal Simulations

Figure 9 shows the zonal mean zonal wind and temperature from the seasonal simulations for the CTL and SOP experiments, which are calculated by averages of five-member ensembles for the boreal winter (DJF) from 2013 to 2014. The seasonal mean states during the selected period are shown to be similar to climatology under the normal SSTs. The biases of the wind and temperature shown by shading for the CTL experiment in Figures 9a and 9c are computed against the FNL data. The differences of the wind and temperature between the two experiments, which are statistically significant at the 95% confidence level, are shown by shading in Figures 9b and 9d. In both experiments, the structures of zonal mean zonal wind and temperature generally agree well with those in the FNL reanalysis data, although the stratospheric easterly and westerly jets (subtropical tropospheric jets) in both hemispheres are slightly weaker (stronger) compared with those of the reanalysis data, and the corresponding temperature biases are shown. A distinct difference between the two experiments appears in the winter stratospheric polar region with the reduced easterly biases (i.e., stronger polar night jet) in the SOP experiment, which correspond to the reduced warm biases in that region via the thermal wind relationship. The strengthened polar night jet in the SOP experiment is mainly due to the GWD in the winter stratosphere being reduced by considering the

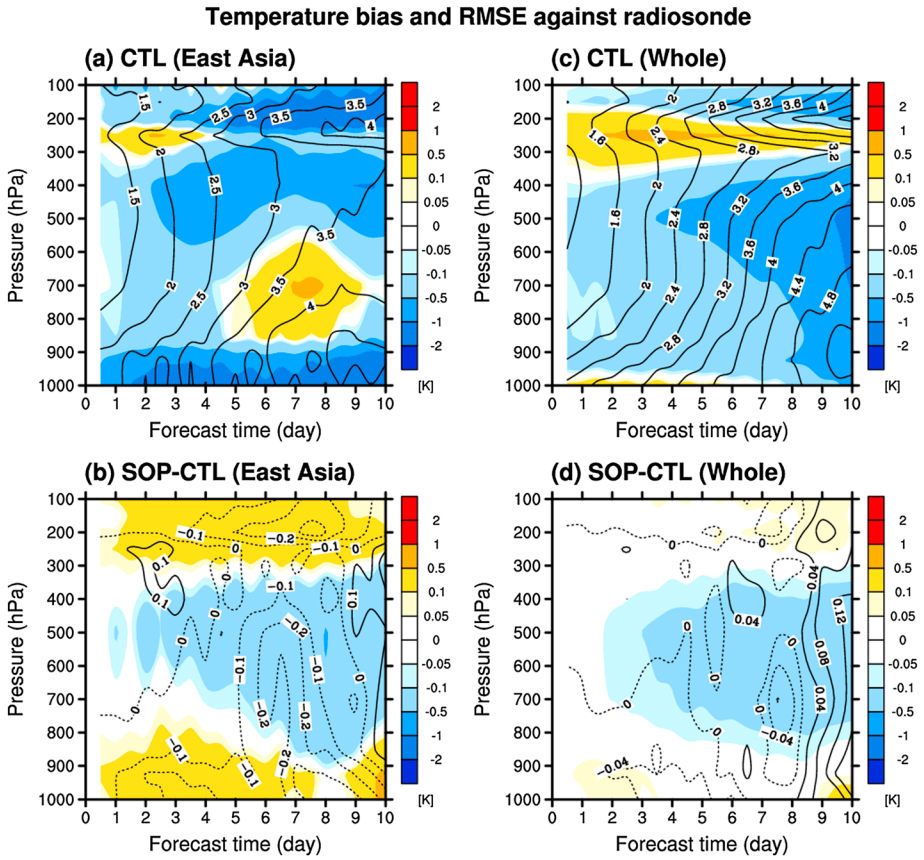

Figure 7. Time-pressure cross sections of the biases (shaded) and RMSEs (contours) of the temperature computed against the radiosonde data averaged over (a, b) East Asia and (c, d) globally from the (top) CTL experiment and the (bottom) differences in bias and RMSE between the SOP and CTL experiments for February 2014.

orographic anisotropic effects. The skill scores (RMSE and pattern correlations) are improved for the zonal mean zonal wind and temperature by updating the SOP.

Additionally, the 500 hPa height eddies (i.e., stationary eddies), which are used to validate the general ability of models, are compared between the two experiments, and overall improvements are observed in the SOP experiment. The pattern correlations with the FNL data of the simulated eddies are 0.70 and 0.77 for the CTL and SOP experiments, respectively. There is little difference in the precipitation between the two experiments (not shown).

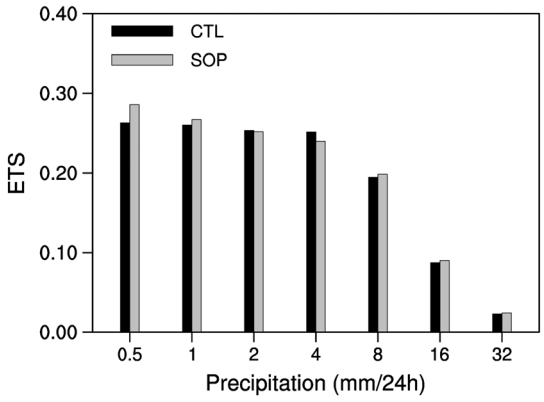

Figure 8. Statistical skill of the equivalent threat scores (ETS) calculated against rain gauge observations over South Korea for 1 to 5 day forecasts from the CTL and SOP experiments during the period of February 2014.

4. Summary and Conclusions

In this study, we have updated the SOP by including the effects of the orographic anisotropy and FBD and examined its impact on short- and medium-range forecasts and seasonal simulations from the GRIMs-GMP. To include the effects of orographic anisotropy, an orographic statistic, OD, is introduced according to *Kim and Doyle* [2005], and the formulations for the OGWD parameterization are modified with the OD. The FBD parameterization generally follows the study of *Kim and Doyle* [2005], except for the height of

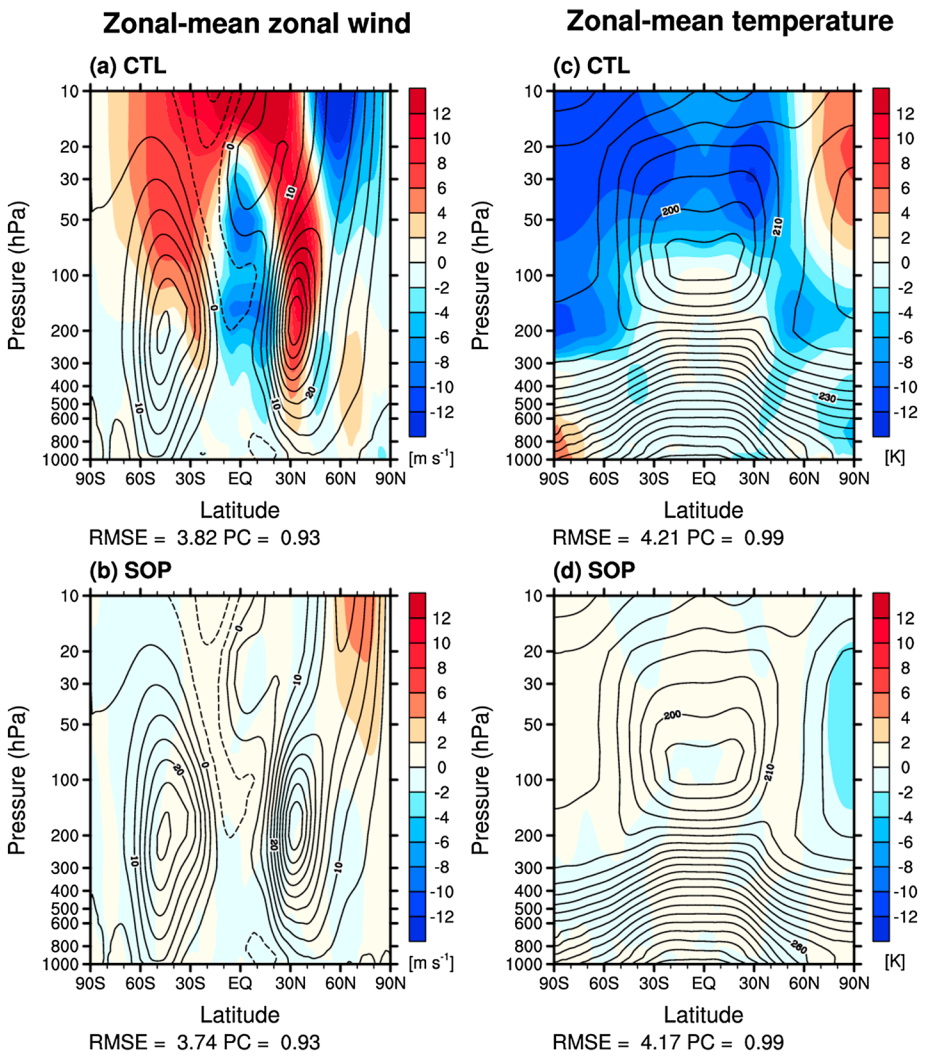

Figure 9. Five-member ensemble averages of the zonal mean (a, b) zonal wind and (c, d) temperature from the (top) CTL and (bottom) SOP experiments (contours) and the (top) biases in the CTL experiment computed against the FNL data and (bottom) the differences between the SOP and CTL experiments (shaded) for DJF 2013–2014. The difference fields are statistically significant at the 95% confidence level.

the blocked layer (h_B) and the bulk drag coefficient (C_d). The h_B is determined by comparing the potential and kinetic energies according to the dividing streamline theory, with the blocked layer occurring when the potential energy exceeds the kinetic energy. The C_d is calculated as a function of the OD by including the orographic anisotropy, as in *Lott and Miller* [1997].

To investigate the impact of the updated SOP on the short- and medium-range forecasts and seasonal simulations, two experiments are performed using the model with original (CTL experiment) and updated (SOP experiment) SOPs. Because the effects of SOP are significant mainly in winter, we focus on high-impact weather events over South Korea during the boreal winter. For the short-range forecasts, a heavy snowfall event over Korea on 4 January 2010, is selected, and the impacts of the updated SOP on the synoptic fields and precipitation over East Asia are investigated by comparing the SOP and CTL results. For the medium-range forecasts, 28-member ensembles of 10 day forecasts are performed every 00:00 UTC for February 2014, when an anomalously long-lasting heavy snowfall event over South Korea occurred, and the synoptic features and precipitation of the CTL and SOP experiments are statistically evaluated based on the forecast skills computed against the radiosonde data and rain gauge observations, respectively. The seasonal simulations consisting of five-member ensembles are performed for DJF 2013–2014 when the seasonal mean states

for boreal winter are shown to be similar to climatology under the normal sea surface temperatures (SSTs), and the impacts of the updated SOP on the seasonal predictability of zonal mean zonal wind and temperature, stationary eddy, and precipitation are examined.

When the SOP is updated, the CTL and SOP experiments comparison reveals that

1. The orographic drag noticeably increases because of the additional flow-blocking drag in the low troposphere.
2. The enhanced orographic drag directly weakens the wind in the low troposphere and indirectly improves the temperature and mass fields.
3. The snowfall overestimation over Korea is improved by the reduced heat fluxes from the surface due to the decreased turbulent exchange coefficients, which result from the weakened wind near the surface.
4. The short-range forecast improvements are robust regardless of the model's horizontal resolution.
5. The skills of the wind speed and temperature for the medium-range forecasts are improved in the low troposphere globally and for East Asia while both positive and negative effects appear indirectly in the middle-upper troposphere.
6. The statistical skill for the precipitation is mostly improved due to the improvements in the synoptic fields.
7. The improvements in the seasonal simulations are found throughout the troposphere and stratosphere during boreal winter.

As mentioned in 1, the changes in the orographic drag are mainly caused by the additional parameterization of the FBD near the surface, while the changes in the GWD, mostly associated with the orographic anisotropy, are not as significant in the troposphere. Nevertheless, the forecast improvements are noticed for the whole troposphere, possibly due to the interactions of the modified orographic drag with forcing terms from other physical and dynamical processes [e.g., *Kim*, 2007]. However, the GWD in the winter stratosphere from the seasonal simulations is significantly reduced by considering the orographic anisotropy; thus, the weak polar night jet shown in the CTL experiment is strengthened (improved) by the reduced GWD in the SOP experiment. The update of the height of the block layer (h_B) in the FBD parameterization produces more drag and leads to better forecasts in the low troposphere than when the original h_B is used. It is found that the forecasts for the East Asia are less sensitive to the update of the bulk drag coefficient (C_d).

The future work will involve a more detailed investigation of not only the seasonal, short-range, and medium-range forecasts but also climate simulations for the whole atmosphere considering the interactions with other wave forcing terms (i.e., nonorographic GWD, planetary wave forcing).

Acknowledgments

The authors would like to thank the anonymous reviewers for their contribution to the paper, Jung-Eun Esther Kim for the bug check, and the support of the KIAPS Forecasts Verification team, particularly Ju-Won Lee and Kyung-Hee Seol. This work has been carried out through the research and development project on the development of the global numerical weather prediction systems of the KIAPS funded by the Korea Meteorological Administration (KMA). The NCEP FNL and GFS analysis data are available from the Computational Information Systems Laboratory (CISL) Research Data Archive (RDA) (http://rda.ucar.edu/datasets/ds083.2/) and the NCEP Environmental Modeling Center (ENC) (ftp://ftp.ncep.noaa.gov/pub/data/nccf/com/gfs/prod), respectively. The radiosonde data are available from KMA and were processed using the KIAPS Package for Observation Processing (KPOP).

References

Alexander, M. J., et al. (2010), Recent developments in gravity-wave effects in climate models and the global distribution of gravity-wave momentum flux from observations and models, *Q. J. R. Meteorol. Soc.*, *136*, 1103–1124.

Batchelor, G. K. (1967), *An Introduction to Fluid Mechanics*, 615 pp., Cambridge Univ. Press, Cambridge, U. K.

Boer, G. J., N. A. McFarlane, R. Laprise, J. D. Henderson, and J.-P. Blanchet (1984), The Canadian Climate Centre spectral atmospheric general circulation model, *Atmos. Ocean*, *22*, 397–429.

Etling, D. (1989), On atmospheric vortex streets in the wake of large islands, *Meteorol. Atmos. Phys.*, *41*, 157–164.

Gregory, D., G. J. Shutts, and J. R. Mitchell (1998), A new gravity-wave-drag scheme incorporating anisotropic orography and low-level wave breaking: Impact upon the climate of the UK Meteorological Office Unified Model, *Q. J. R. Meteorol. Soc.*, *124*, 463–493.

Hong, S.-Y., J. Choi, E.-C. Chang, H. Park, and Y.-J. Kim (2008), Lower-tropospheric enhancement of gravity wave drag in a global spectral atmospheric forecast model, *Weather Forecasting*, *23*, 523–531.

Hong, S.-Y., et al. (2013), The Global/Regional Integrated Model system (GRIMs), *Asia-Pac. J. Atmos. Sci.*, *49*(2), 219–243.

Kanamitsu, M. (1989), Description of the NMC global data assimilation and forecast system, *Weather Forecasting*, *4*, 335–342.

Kanamitsu, M., et al. (2002), NCEP dynamical seasonal forecast system 2000, *Bull. Am. Meteorol. Soc.*, *83*, 1019–1037.

Kim, Y.-J. (1996), Representation of subgrid-scale orographic effects in a general circulation model: Part I. Impact on the dynamics of a simulated January climate, *J. Clim.*, *9*, 2698–2717.

Kim, Y.-J. (2007), Balance of drag between the middle and lower atmospheres in a global atmospheric forecast model, *J. Geophys. Res.*, *112*, D13104, doi:10.1029/2007JD008647.

Kim, Y.-J., and A. Arakawa (1995), Improvement of orographic gravity wave parameterization using a mesoscale gravity wave model, *J. Atmos. Sci.*, *52*, 1875–1902.

Kim, Y.-J., and J. D. Doyle (2005), Extension of an orographic-drag parameterization scheme to incorporate orographic anisotropy and flow blocking, *Q. J. R. Meteorol. Soc.*, *131*, 1893–1921.

Kim, Y.-J., S. D. Eckermann, and H.-Y. Chun (2003), An overview of the past, present and future of gravity-wave drag parametrization for numerical climate and weather prediction models, *Atmos. Ocean*, *41*, 65–98.

Lim, K.-S., S.-Y. Hong, J.-H. Yoon, and J. Han (2014), Simulation of the summer monsoon rainfall over East Asia using the NCEP GFS cumulus parameterization at different horizontal resolutions, *Weather Forecasting*, *29*, 1143–1154.

Lott, F., and M. J. Miller (1997), A new subgrid-scale orographic drag parameterization: Its formulation and testing, *Q. J. R. Meteorol. Soc.*, *123*, 101–127.

McFarlane, N. A. (1987), The effect of orographically excited gravity-wave drag on the general circulation of the lower stratosphere and troposphere, *J. Atmos. Sci.*, *44*, 1775–1800.

Miller, M. J., T. N. Palmer, and R. Swinbank (1989), Parameterization and influence subgrid-scale orography in general circulation and numerical weather prediction models, *Meteorol. Atmos. Phys.*, *40*, 84–109.

Palmer, T. N., G. J. Shutts, and R. Swinbank (1986), Alleviation of a systematic westerly bias in general circulation and numerical weather prediction models through an orographic gravity-wave drag parameterization, *Q. J. R. Meteorol. Soc.*, *112*, 1001–1039.

Reynolds, R. W., T. M. Smith, C. Liu, D. B. Chelton, K. S. Casey, and M. G. Schlax (2007), Daily high-resolution-blended analyses for sea surface temperature, *J. Clim.*, *20*, 5473–5496.

Scinocca, J. F., and N. A. McFarlane (2000), The parameterization of drag induced by stratified flow over anisotropic topography, *Q. J. R. Meteorol. Soc.*, *126*, 2353–2393.

Snyder, W. H., R. S. Thompson, R. E. Eskridge, R. E. Lawson, I. P. Castro, J. T. Lee, J. C. R. Hunt, and Y. Ogawa (1985), The structure of strongly stratified flows over hills: Dividing streamline concept, *J. Fluid Mech.*, *152*, 249–288.

Webster, S., A. R. Brown, D. R. Cameron, and C. P. Jones (2003), Improvements to the representation of orography in the Met Office Unified Model, *Q. J. R. Meteorol. Soc.*, *129*, 1989–2010.

Zadra, A., M. Roch, S. Laroche, and M. Charron (2003), The subgrid-scale orographic blocking parameterization of the GEM model, *Atmos. Ocean*, *41*, 155–170.

Zhong, S., and Z. Chen (2015), Improved wind and precipitation forecasts over South China using a modified orographic drag parameterization scheme, *J. Meteorol. Res.*, *29*(1), 132–143.